Arf6, JIP3, and dynein shape and mediate macropinocytosis

Chad D. Williamson[a,b] and Julie G. Donaldson[a,*]
[a]Cell and Developmental Biology Center, National Heart, Lung and Blood Institute, and [b]Cell Biology and Neurobiology Branch, Eunice Kennedy Shriver Institute of Child Health and Human Development, National Institutes of Health, Bethesda, MD 20892

ABSTRACT Macropinocytosis is an actin-driven form of clathrin-independent endocytosis that generates an enlarged structure, the macropinosome. Although many studies focus on signaling molecules and phosphoinositides involved in initiating macropinocytosis, the commitment to forming a macropinosome and the handling of that membrane have not been studied in detail. Here we show in HT1080 cells, a human fibrosarcoma cell line, a requirement for microtubules, dynein, the JIP3 microtubule motor scaffold protein, and Arf6, a JIP3 interacting protein, for the formation and inward movement of the macropinosome. While actin and myosin II also play critical roles in the formation of ruffling membrane, microtubules provide an important tract for initiation, sealing, and transport of the macropinosome through the actin- and myosin-rich lamellar region.

INTRODUCTION

Macropinocytosis is a conserved form of endocytosis generated through actin ruffles and protrusions at the plasma membrane (PM) that fold over and seal causing large vesicles (>0.2 μm in diameter) to enter the cell interior (Swanson, 2008; Kerr and Teasdale, 2009; Buckley and King, 2017). In mammalian cells it can be transiently induced with growth factor stimulation and can involve activities of Ras (Bar-Sagi and Feramisco, 1986; Porat-Shliom et al., 2008), PI3 kinase (Araki et al., 1996; Amyere et al., 2000), Src (Veithen et al., 1996), Rac (West et al., 1989), and Rab5 and Arf6 (Frittoli et al., 2008; Porat-Shliom et al., 2008). Some immune cells, such as immature dendritic cells and macrophages, exhibit constitutive macropinocytosis. They use this as a means of sampling extracellular

material for antigens to process and present on their cell surfaces. In *Dictyostelium*, constitutive macropinocytosis is used to take in large amounts of fluid, providing a source of nutrients (Hacker et al., 1997). Ras-transformed cancer cells also exhibit constitutive macropinocytosis (Bar-Sagi and Feramisco, 1986; Porat-Shliom et al., 2008) and recently it was shown that this activity can provide a source of nutrients for tumor growth in animals (Commisso et al., 2013). The use of macropinocytosis for nutrition in cancer cells also offers another avenue for therapeutic intervention (Ha et al., 2016). Overall, the use of macropinocytosis to obtain nutrients may be an ancient and widely observed trait of eukaryotic cells.

Constitutive macropinocytosis can be induced in HeLa and Cos7 cells on expression of active forms of H-Ras (Porat-Shliom et al., 2008; Zoncu et al., 2009). These macropinosomes form from and utilize membrane components, including Arf6, associated with clathrin-independent endocytosis (CIE) (Porat-Shliom et al., 2008). These findings led us to propose that macropinocytosis is a stimulated form of CIE that produces a large incoming endosome (Donaldson et al., 2009). As we have been following the sorting of a number of CIE cargo proteins on endosomes (Eyster et al., 2009; Maldonado-Baez et al., 2013), we wondered whether cells exhibiting macropinocytosis might provide an opportunity to follow endosomal trafficking and further explore the role of actin and myosin in macropinosome formation.

Here we examined how the PM enters cells during macropinocytosis. In addition to the requirement for actin and myosin contractility, we uncovered a surprising requirement for microtubules, dynein motors, and the Arf6 effectors, the Jun kinase interacting proteins (JIP3/JIP4) scaffold proteins, for macropinocytosis to occur. This
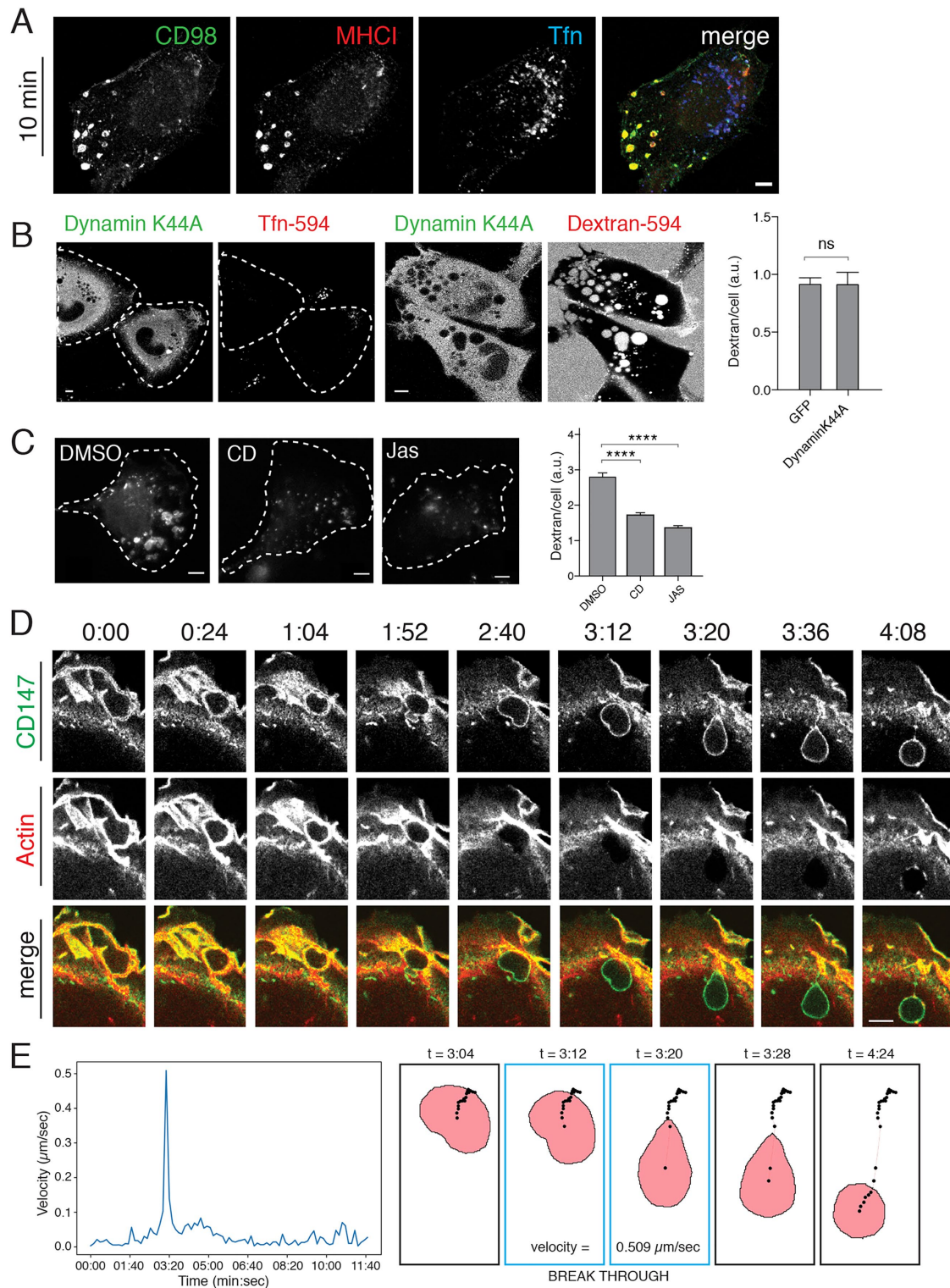
FIGURE 1: Actin-coated macropinosomes contain CIE cargo proteins. (A) HT1080 cells were incubated with serum-free media for 30 min followed by overlay with monoclonal antibodies against CD98 (green) and MHCI (red), and Alexa-633-transferrin (Tfn) in serum-free media for 10 min at 37°C to allow internalization. Cells were washed with low pH solution, fixed, and immunolabeled with fluorescent secondary antibodies. (B) HT1080 cells expressing dynamin-K44A-GFP were incubated with Tfn-594 or dextran-594 for 20 min prior to fixation and direct imaging. The amount of internalized dextran per cell was quantified by Metamorph in cells expressing GFP or DynaminK44A-GFP (at least 87 GFP-positive cells per condition). An unpaired t test with Welch's correction was used for comparison of conditions, p = 0.9868 (C) HT1080 cells were pretreated with 100 nM cytochalasin D, 500 nM jasplakinolide, or DMSO for 15 min at 37°C prior to addition of dextran-594 and incubation for 20 min. Cells were then fixed and the mean dextran fluorescence of at least 196 individual cells per condition in a single matched experiment is shown (± SEM). Experiments were repeated three times with similar phenotypes. An ordinary one-way analysis of variance (ANOVA) was used to compare drug-treated conditions to the

machinery is required for generation of the macropinosome and transport past the lamellar region for subsequent cargo sorting in the cell interior.

RESULTS

Actin-coated macropinosomes contain CIE cargo proteins

HT1080 cells are a human fibrosarcoma cell line (HT1080) that exhibits constitutive macropinocytosis due to expression of an active mutation in N-Ras. We examined the cargo contents of the macropinosomes entering HT1080 cells to see whether they contained CIE cargo proteins as was seen previously in Ras-transfected HeLa cells (Porat-Shliom et al., 2008). To do this, cells were incubated with antibodies to CD98 and major histocompatibility class I (MHCI) together with labeled transferrin to allow their internalization, followed by removal of surface antibodies, fixation, and detection of internalized antibodies. After 10 min, CD98 and MHCI were both observed in large (1–2 μm) peripheral endosomes that lacked transferrin, which enters cells by clathrin-mediated endocytosis (CME) and was present in a collection of smaller juxtanuclear endosomes (Figure 1A). Consistent with macropinocytosis being a form of CIE, expression of the K44A mutant of dynamin, known to block (CME) (van der Bliek et al., 1993), did not inhibit macropinocytosis as observed by imaging cells and measured by fluorescent dextran uptake (Figure 1B). The internalization of fluorescent dextran, a fluid marker that can enter cells by all endocytic mechanisms, can be used to quantify macropinocytosis. By contrast, transferrin internalization was impaired in cells expressing the K44A mutant of dynamin (Figure 1B). Macropinocytosis is an actin-dependent process (Swanson, 2008). We found that treatment of cells with low concentrations of the actin-disrupting, drug cytochalasin D (100 nM), or the actin stabilizing drug, jasplakinolide, resulted in inhibition of macropinocytosis, quantified by measuring the amount of fluorescent dextran internalized into the cells (Figure 1C). Even lower doses of drugs affecting actin turnover showed dramatic effects on membrane ruffling, blocking macropinocytosis (unpublished data).

Since these large incoming macropinosomes arise from actin–filament-rich ruffling regions of the PM, we examined the entry of CD147, another CIE cargo protein, in cells expressing mApple-F-tractin to label actin filaments (Johnson and Schell, 2009; Beach et al., 2014) (Figure 1D and Supplemental Movie 1). Actin filaments can be observed in the lamellar region and also coating the newborn macropinosome, labeled with cargo, still in the lamellae. We noticed that once past the lamellar region, the macropinosomes had lost their actin coat and were propelled into the cell interior (Figure 1D and Supplemental Movie 1). We also noticed deformation or squeezing of the macropinosome as it moved through the lamellar region and out into the cell interior (Figure 1D, 1:52, 2:40, and 3:12 timepoints). The movement of the macropinosome shown in Figure 1D was tracked through time using Nikon Elements Software (NIS). Displacement of the centroid of the macropinosome was measured from frame-to-frame (8-s intervals) and plotted as macropinosome velocity over time (Figure 1E, graph). Illustrations in Figure 1E show the progression of the centroid track (black dots) through time. A snapshot of the macropinosome region, as defined by the NIS software, is also shown for the indicated time points to highlight fidelity of the macropinosome shape compared with the original micrographs in Figure 1D. The macropinosome moves slowly while surrounded by actin in the lamella and while displaying 90° angle deformations, which seems to correspond with movement through the actin arc at the base of the lamella. A spike in macropinosome velocity (0.509 μm/s) is seen when the marcopinosome breaks free into the cell interior.

The dense network of actin in the lamellopodia and the evidence of substantial actin retrograde flow acting on the macropinosome during movement through the lamella (see Supplemental Movie 1) led us to ask whether nonmuscle myosin II could be involved in this process as has been observed by others (Araki et al., 2003; Jiang et al., 2010). First, we examined the localization of endogenous myosin IIA and B by immunofluorescence. Myosin IIA was present in the lamella and at the leading edge where it colocalized with F-actin, labeled with phalloidin (Figure 2A). By contrast, myosin IIB predominantly localized at the actin arcs at the base of the lamella (Figure 2B, arrowhead). Fixed images of cargo-labeled and deformed macropinosomes showed myosin IIA coating on the part of the macropinosome still in the lamellae but not present on the part of the macropinosome on the other side of the actin arc barrier (Figure 2C, arrowhead). Myosin IIB, by contrast, defined the barrier through which the macropinosome was being squeezed (Figure 2D, arrowhead). This differential localization of the two myosins early in macropinosome development led us to examine whether myosin II activity was required for macropinocytosis and macropinosome maturation by treating the cells with blebbistatin, an inhibitor of myosin II (Kovacs et al., 2004). Blebbistatin treatment inhibited macropinocytosis, as measured by dextran uptake, (Figure 2, E and F), indicating that myosin II activity was required for macropinosome formation or maturation. It is worth noting that we initially encountered variable results with blebbistatin when the drug was diluted into room temperature media, with replicate experiments often showing no effects on macropinocytosis. Other investigators have reported that this compound can readily precipitate out of solution, especially if diluted into cool or RT media (Swift et al., 2012). Adopting the strict practice of preheating media aliquots and stock blebbistatin solutions to 37°C prior to use eliminated this variability and clearly revealed a positive effect of myosin II activity on macropinocytosis. It thus appears as though both actin and myosin II motors are required to form the macropinosome and to deform it as it gets pushed through the actin arc.

Microtubules and dynein are required for macropinocytosis

The propulsion of macropinosomes into the cell interior after clearing the actin-rich lamellar region (shown in Supplemental Movie 1)

DMSO condition. **** $p < 0.0001$. Sample images corresponding to each condition are shown; cells are outlined with white dotted lines. (D) HT1080 cells expressing mApple-F-tactin (red) to label actin filaments were incubated with Alexa488–conjugated primary antibodies against CD147 for 1 h prior to imaging. Membrane ruffling and macropinocytosis were followed in live-cell imaging over the course of 22 min (see Supplemental Movie 1). Stills from Supplemental Movie 1 show sealing of actin-positive lamellar membranes into a nascent macropinosome, maturation of the macropinosome through the actin-rich lamellae, loss of uniform actin signal from the limiting membrane of the macropinsome as it enters the cell interior, and subsequent sorting of endogenous CD147. (E) Displacement of the centroid of the macropinosome shown in D was measured from frame to frame, in Nikon Elements Software, as it enters the cell and passes through the actin arc into the cell interior. Velocity over time is plotted with breakthrough occuring between 3:12 and 3:20 with a velocity of 0.509 μm/s. Illustrations show the progression of the centroid track (black dots) through time, along with a snapshot of the macropinosome ROI at indicated time points. Bars, 5 μm.
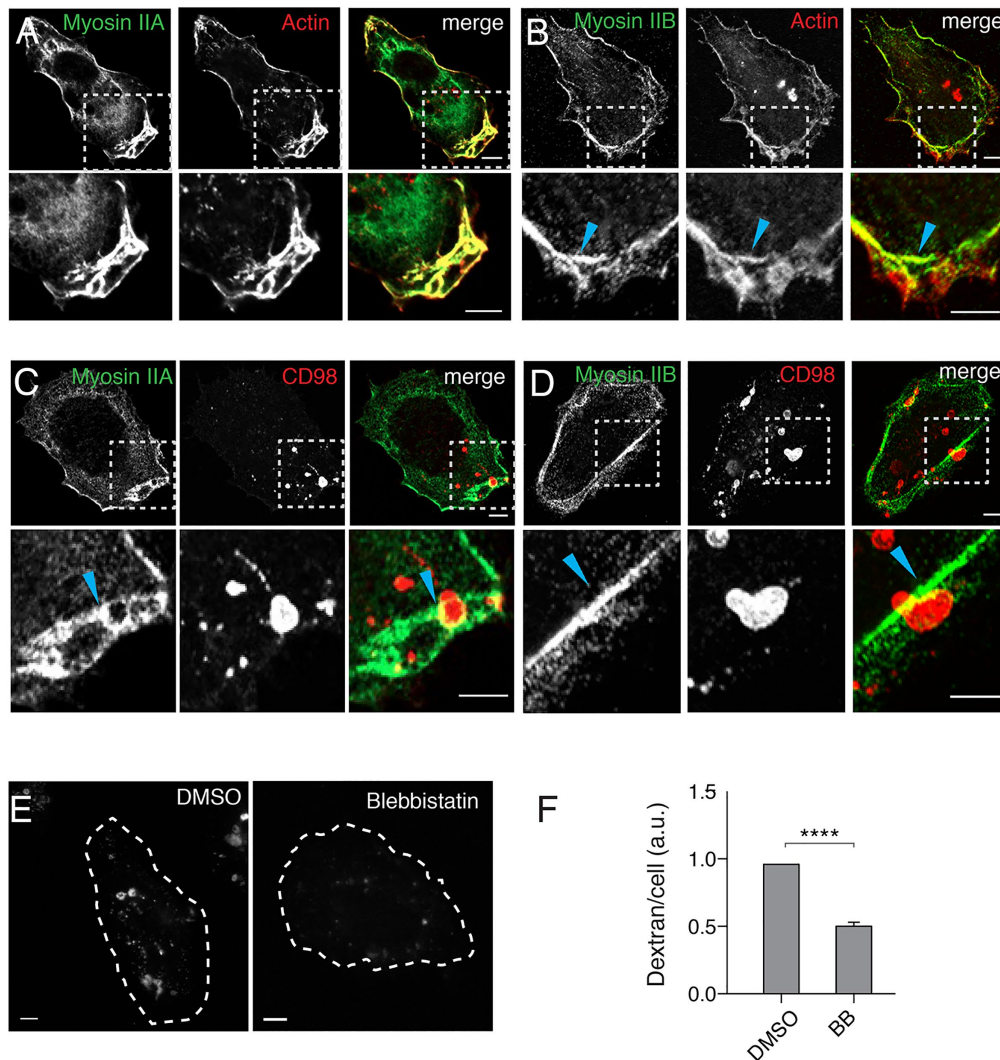
FIGURE 2: Myosin IIA and IIB are distinctly localized to the lamella and myosin activity is required for macropinocytosis. (A, B) HT1080 cells were fixed and labeled with antibodies to myosin IIA (A) or myosin IIB (B) and rhodamine-phalloidin to label actin. (C, D) HT1080 cells were incubated with antibodies against CD98 for 30 min prior to removal of surface antibody, fixed, and labeled with antibodies to myosin IIA (C) or IIB (D). For A–D, boxed regions are enlarged and shown below. (E, F) HT1080 cells were pretreated with either 50 µM blebbistatin or DMSO vehicle for 30 min prior to the addition of dextran (dextran-594 in E, dextran-647 in F) and further incubation for 20 min. Bar graph (F) shows the geometric mean dextran fluorescence measured by flow cytometry, reported as a fraction of DMSO control, from at least three experiments (100,000 cells were counted per experiment). Error bars represent $\pm$ SD. An unpaired t test with Welch's correction was used for comparison of conditions. ****$p < 0.0001$. Images corresponding to typical dextran fluorescence under each condition are shown, cells are outlined with white dotted lines. Bars, 5 µm.

suggests the possibility that microtubules and microtubule motors may be important for macropinosome transport. We examined whether peripheral microtubules, or so-called pioneering microtubules (Waterman-Storer and Salmon, 1997), might extend into the lamellar region and facilitate macropinosome movement. HT1080 cells were cotransfected with a green fluorescent protein (GFP)-fused ensconsin microtubule-binding domain, EMTB-3xGFP, to label microtubules (Faire et al., 1999) and mApple-F-tractin to label actin filaments. Live imaging of these cells showed some microtubules reaching out into the lamellar regions and making contact with incoming macropinosomes that were coated with actin at early times (Figure 3A and Supplemental Movie 2). Then, around time 6:49, actin is shed from the macropinosome, which is now visible as a black hole in the 488/GFP channel and microtubules can be

observed in contact with the macropinosome (Figure 3A and Supplemental Movie 2). To examine whether microtubules in the lamellar region were important for macropinocytosis, we treated cells with nocodazole to inhibit microtubule polymerization and then assessed their ability to take in dextran. Cells treated with nocodazole had a drastic decrease in the amount of fluid internalization (Figure 3B). This effect was also observed with other inhibitors of microtubule assembly, colcemid and vinblastine (Figure 3C).

We also examined the effect of microtubule depolymerization on the cells using live-cell imaging. HT1080 cells were incubated with 488–conjugated antibody to CD147 to label the surface and then the cells were imaged in the absence or the presence of nocodazole. In control (dimethyl sulfoxide [DMSO]-treated) cells, active ruffling and macropinosome formation was observed in the lamellar region
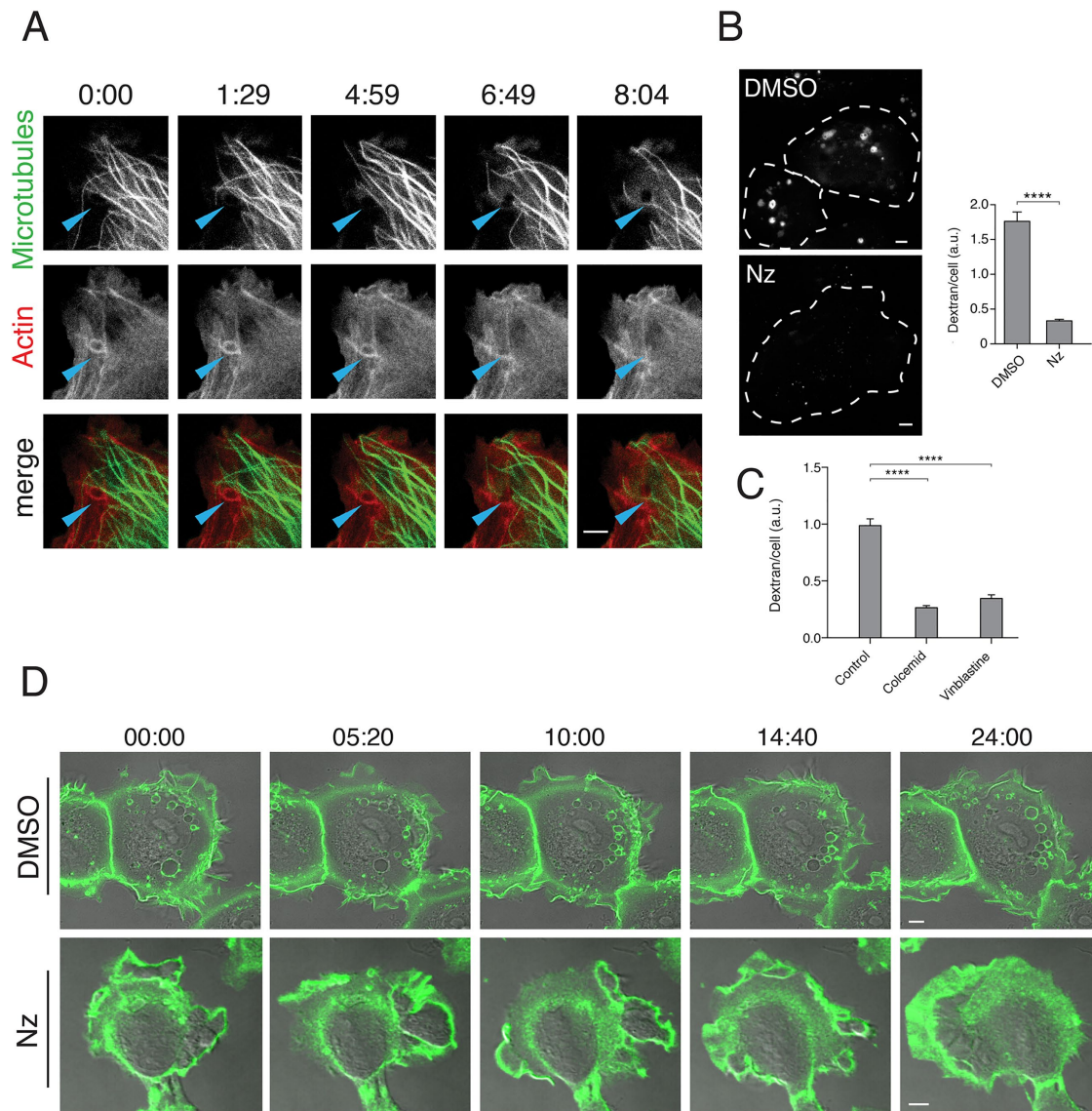
FIGURE 3: Microtubules are critical for macropinosome formation. (A) HT1080 cells expressing EMTB-3xGFP (green) and mApple-F-tractin (red) to label microtubules and actin, respectively, were imaged live (Supplemental Movie 2). In selected frames, arrowheads highlight a nascent macropinosome as it moves through the lamella into the cell interior. (B) HT1080 cells were pretreated with either 10 µg/ml nocodazole or DMSO for 30 min prior to addition of dextran-594 and incubation for 20 min. Images of cells from each condition are shown, cells outlined with white dotted lines. Bar graphs show the average (± SEM) dextran fluorescence from 150 individual cells per condition in a single matched experiment. Experiments were repeated three times with similar phenotypes. An unpaired t test with Welch's correction was used for comparison of conditions. **** $p < 0.0001$. (C) HT1080 cells were pretreated with 5 µM cholcemid for 1 h 600 nM vinblastine for 30 min, or matched vehicle prior to addition of dextran-594 and incubation for 20 min. Bar graphs show the average (± SEM) dextran fluorescence of 200 cells per condition in a single matched experiment. An ordinary one-way ANOVA was used to compare drug-treated conditions to the vehicle control. ****p value < 0.0001. (D) HT1080 cells were incubated with Alexa 488–conjugated antibody to CD147 for 1 h. Cells were then imaged live after 20 min of pretreatment with either DMSO (see Supplemental Movie 3) or 10 µg/ml nocodazole (see Supplemental Movie 4); stills from these movies are shown. Bars, 5 µm.

(Figure 3D, top row, and Supplemental Movie 3). By contrast, cells treated with nocodazole for 20 min exhibited smooth, uniform lamellar ruffling around the cell edges and the absence of macropinosome formation (Figure 3D, bottom row, and Supplemental Movie 4). Lamellar ruffling without productive macropinosome formation was a striking, and surprising, phenotype. We decided to test whether Ras-induced macropinocytosis, previously reported in HeLa and Cos cells by expression of active forms of Ras (Porat-Shliom

et al., 2008), also required microtubules. HeLa cells expressing N-RasG12V took up more dextran than cells expressing GFP alone, and this effect was inhibited with nocodazole treatment (Supplemental Figure S1), consistent with a requirement for microtubules in Ras-induced macropinocytosis in HeLa cells.

Macropinosomes that form in the periphery move through the lamellae by actin retrograde flow and myosin II motor activity, followed by movement into the cell interior (see Figure 1D). The
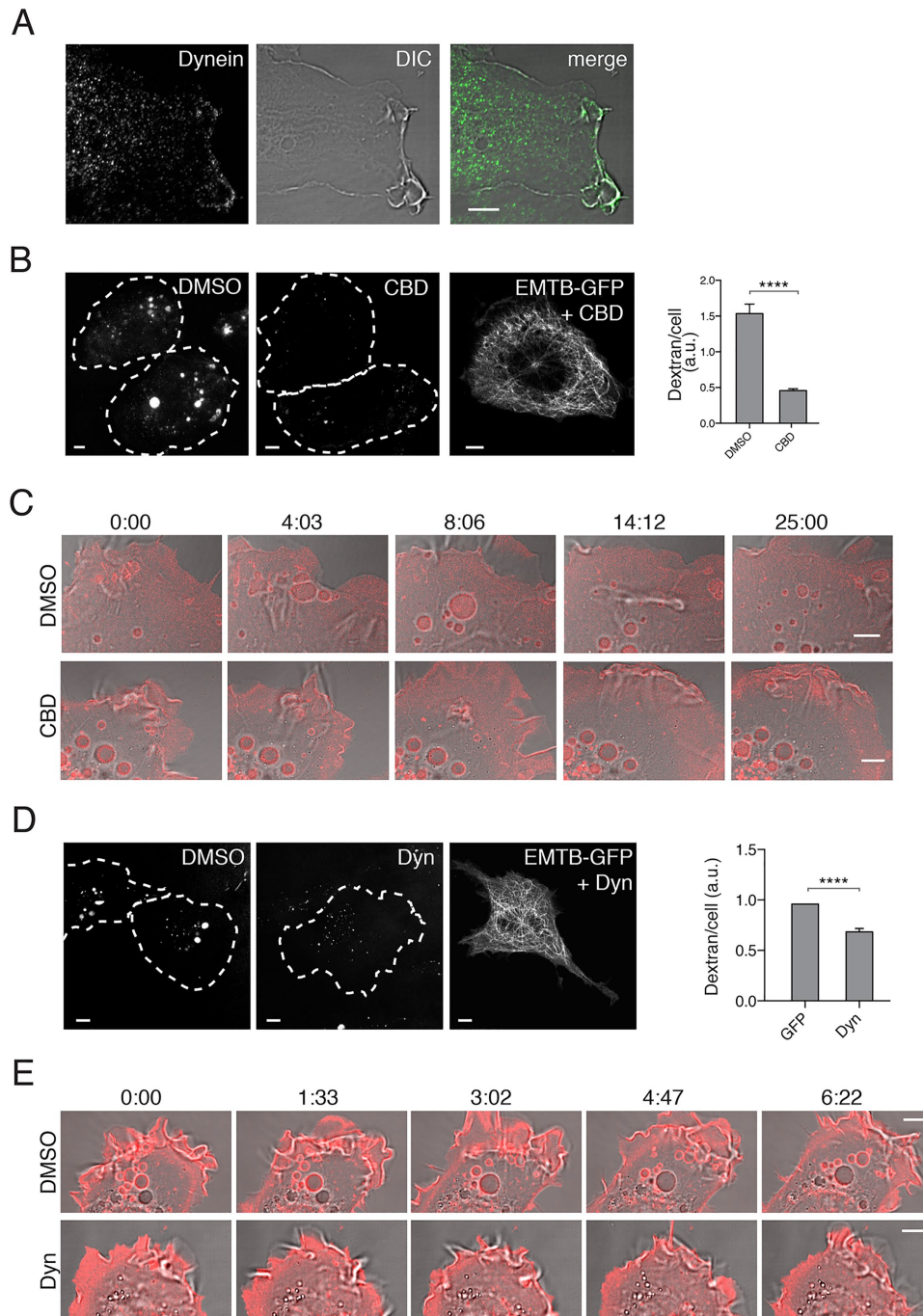
FIGURE 4: Dynein motor activity is required for macropinocytosis. (A) HT1080 cells were imunolabeled with antibody to cytosolic dynein. (B) HT1080 cells were pretreated with either 50 μM Ciliobrevin D (CBD) or DMSO vehicle for 30 min before addition of dextran-594 and incubated for 20 min. Images of cells under each condition are shown, cells are outlined with white dotted lines. HT1080 cell expressing EMTB-3xGFP and treated with CBD is shown, revealing intact microtubules throughout the cell in the presence of this drug. Bar graphs show the average (± SEM) dextran fluorescence from 150 individual cells per condition in a single matched experiment. Experiments were repeated three times with similar phenotypes. An unpaired t test with Welch's correction was used for comparison of conditions. ****p value < 0.0001. (C) HT1080 cells expressing farnesyl-RFP to label the cell surface were pretreated with 50 μM Ciliobrevin D (CBD) or DMSO for 30 min and then imaged live; stills from that movie are shown. Nascent macropinosomes can be seen forming in DMSO treated cells, while CBD-treated cells have ruffling membranes but are impaired at forming macropinosomes. (D) HT1080 cells were pretreated with 40 μM Dynarrestin (Dyn) or DMSO for 1 h prior to addition of dextran-594 and incubated for 20 min. Images of cells under each condition are shown; cells are outlined with white dotted lines. HT1080 cell expressing EMTB-3xGFP and treated with Dyn is shown, revealing intact microtubules throughout the cell in the presence of this drug. HT1080 cells were treated as above but incubated with dextran-647 for 20 min prior to measuring dextran uptake by flow cytometry. Bar graphs show the geometric mean dextran fluorescence, reported as a fraction of DMSO control, from at least three experiments (100,000 cells were

requirement for microtubules and the inward movement of the macropinosomes suggest the involvement of a minus end–directed dynein motor. Endogenous, cytoplasmic dynein was observed at the PM, in the lamellar regions and associated with forming macropinosomes (Figure 4A). To assess whether dynein motor activity was required for macropinocytosis, we treated cells with Ciliobrevin D, a dynein inhibitor (Roossien et al., 2014), and found that macropinocytosis was indeed inhibited (Figure 4B) even though intact microtubules were still present (see EMTB-GFP in Figure 4B). Live-cell imaging of cells treated with Ciliobrevin showed that lamellar ruffling continued, but as the ruffles attempt to fall back on the membrane to seal the macropinosome, the process appears to be aborted as no new macropinosomes arise from the cell edge (see movie stills in Figure 4C). Furthermore, the macropinosomes present at the start of the movie (time 0) remain static throughout the 25 min in the Ciliobrevin-treated cells (Figure 4C). By contrast, in control cells, macropinosomes continue to enter the cells as existing macropinosomes move inward over the course of the movie (Figure 4C, DMSO).

To lend further support for a role for dynein in macropinocytosis, we treated cells with another inhibitor of dynein, dynarrestin (Hoing et al., 2018). Dynarrestin also inhibited macropinocytosis as evidenced by a decrease in dextran internalization (Figure 4D). Live-cell imaging of cells treated with dynarrestin showed cell surface ruffling but lack of completion of macropinosomes (Figure 4E).

Arf6 and JIP3 are required for macropinocytosis

Having shown a dependence on microtubules and dynein for macropinocytosis in HT1080 cells, we wanted to find cellular components that would connect microtubules to the macropinosome membrane. One type of component we considered were JIP3 and JIP4. JIP3 binds to both kinesin and the p150-glued subunit of dynein (Fu and Holzbaur, 2014). In addition, JIP3 and JIP4 contain a leucine zipper motif that binds to active forms of Arf6 (Isabet et al., 2009; Montagnac et al., 2009). It is thought that Arf6-GTP (guanosine triphosphate) may recruit the JIP to the PM, and depending on subsequent interactions, the JIP may favor kinesin or dynein motor activity (Montagnac et al., 2009; Marchesin et al., 2015). We previously showed that Arf6 activity was required for macropinocytosis in cells expressing active forms of H-Ras (Porat-Shliom et al., 2008). To investigate the involvement of Arf6 and JIP in the HT1080 cells, we examined whether Arf6, JIP3, or JIP4 were required for macropinocytosis. We found that Arf6-GFP was present at the PM and on the peripheral macropinosomes that contained incoming cargo proteins (Figure 5A), whereas expression of the GTP-binding-defective mutant of Arf6, Arf6T27N-GFP, inhibited macropinocytosis (Figure 5, A and B), as was observed in H-Ras-expressing HeLa cells (Porat-Shliom et al., 2008). Furthermore, we found that expression of Rab35, which reduces Arf6-GTP by recruitment of an Arf6 GAP (Chesneau et al., 2012; Chaineau et al., 2013; Dutta and Donaldson, 2015), also led to a decrease in macropinocytosis (Figure 5B), suggesting that active Arf6 is important for macropinocytosis.

Next, we depleted cells of Arf6, JIP3, or JIP4 using small interfering RNA (siRNA) and could show by Western blot with antibodies to Arf6 and JIP4 that they were depleted (Figure 5D).

We did not have reagents to assess JIP3 levels. Depletion of JIP3, and to a lesser extent JIP4, severely inhibited macropinocytosis, as monitored by dextran internalization (Figure 5C). Depletion of Arf6 also led to a decrease in macropinocytosis (Figure 5, C and E), consistent with the effects of expression of Arf6T27N on dextran uptake (Figure 5B). We also saw in live-cell imaging that cells depleted of JIP3 ruffled, but macropinosomes did not form and enter cells efficiently (Figure 5E and Supplemental Movies 5, control, and 6, si JIP3); cells depleted of Arf6 appeared to attempt to form a macropinosome but failed (Figure 5E and Supplemental Movie 7). For both Arf6- and JIP3-depleted cells, macropinosomes were initiated but not completed, similar to what was observed with the dynein inhibitors (see Figure 4, C and E).

JIP3 and JIP4 interact specifically with Arf6 and not with other Arf proteins (Montagnac et al., 2009). The site of interaction between Arf6 and the second leucine zipper motif of JIP4 has been mapped (Isabet et al., 2009; Montagnac et al., 2009) and found to involve the interswitch regions of Arf6. To test whether Arf6 was specifically required for engagement of JIPs for micropinocytosis, we made a mutant of Arf6 (Arf6TKN) containing alterations in this interswitch region that was impaired in JIP3 binding but could still bind to another Arf6 effector, phosphatidyl inositol 4-phosphate 5-kinase (Suzuki et al., 2010). We found that expression of an siRNA-resistant wild-type Arf6 could rescue macropinocytosis in cells depleted of endogenous Arf6 (Figure 6). However, expression of an siRNA-resistant Arf6TKN mutant was not able to rescue macropinocytosis (Figure 6), suggesting that Arf6 engagement with JIP3 was important for macropinocytosis.

Taken together, these findings suggest that Ras-driven macropinocytosis is dependent on actin and myosin for formation and movement through the lamellae but is also dependent on microtubules and dynein motor activity regulated by Arf6 and JIP3/JIP4. It was especially striking that these requirements, like those of dynein motor, were for the initiation and completion of macropinosome closure. In fact, we were surprised that at no point in our study could we discern an accumulation of sealed macropinosomes stuck within the cellular lamellae, limited in the ability to move on into the cell interior. This could be due to the fact that macropinosome closure is linked to the movement through the lamellae and propulsion into the cell interior mediated by microtubules and dynein.

DISCUSSION

Macropinocytosis is a conserved form of endocytosis that has fascinated cell biologists since it was first observed in 1931 (Kerr and Teasdale, 2009). Although the roles of signaling molecules and phosphoinositides in macropinocytosis have been well documented (Swanson, 2008; Bohdanowicz and Grinstein, 2013), here we reveal intriguing aspects of formation and maturation that address how membrane flow and dynamics are controlled. Most striking is the requirement for microtubules and dynein motors for facilitating the formation of and transport of the macropinosome through the actin/myosin lamellar region into the cell interior for subsequent sorting of membrane (see Figure 7). The large size of these incoming macropinosomes allows for unique spatial and temporal resolution of the process from formation to maturation.

counted per experiment). Error bars represent ± SD. An unpaired t test with Welch's correction was used for comparison of conditions. ****p < 0.0001. (E) HT1080 cells expressing GLUT4-mCherry to label the cell surface were pretreated with 40 μM Dynarrestin (Dyn) or DMSO for 1 h and then imaged live; stills from that movie are shown. Nascent macropinosomes can be seen forming in DMSO-treated cells, while Dyn-treated cells have ruffling membranes but are impaired at forming macropinosomes. Bars, 5 μm.
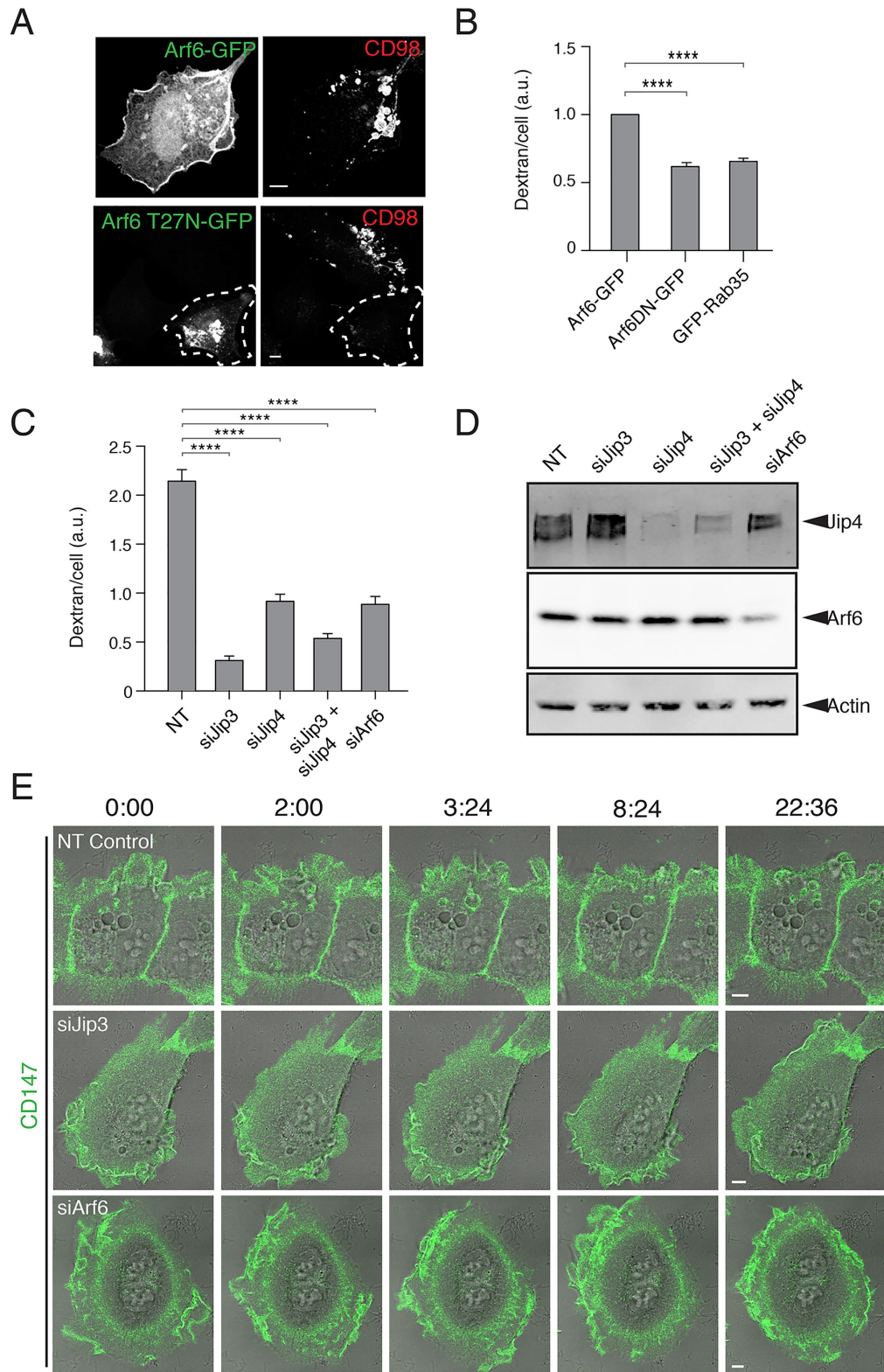
FIGURE 5: Arf6 and JIP3/JIP4 are required for macropinosome formation and maturation. (A) HT1080 cells expressing Arf6-GFP (top) or Arf6T27N-GFP (bottom) were incubated with antibodies to CD98 for 20 min prior to acid wash, fixation, and immunolabeling with fluorophore–conjugated secondary antibodies. (B) HT1080s cells expressing GFP, Arf6T27N-GFP, or GFP-Rab35 were incubated with Dextran-647 for 20 min, and dextran uptake was measured by flow cytometry. Bar graphs show the geometric mean dextran fluorescence of GFP-positive cells, reported as a fraction of Arf6-GFP control, from three separate experiments (GFP-positive cells were gated from a total of 100,000 cells per experiment). An ordinary one-way ANOVA was used to compare groups to the Arf6-GFP control. Error bars represent ± SD. ****p value < 0.0001. Bars, 5 μm. (C) Control HT1080 cells and cells depleted of JIP3, JIP4, JIP3, and JIP4, or Arf6 were incubated for 20 min with dextran-594 and then fixed and imaged. Bar graphs show the average dextran
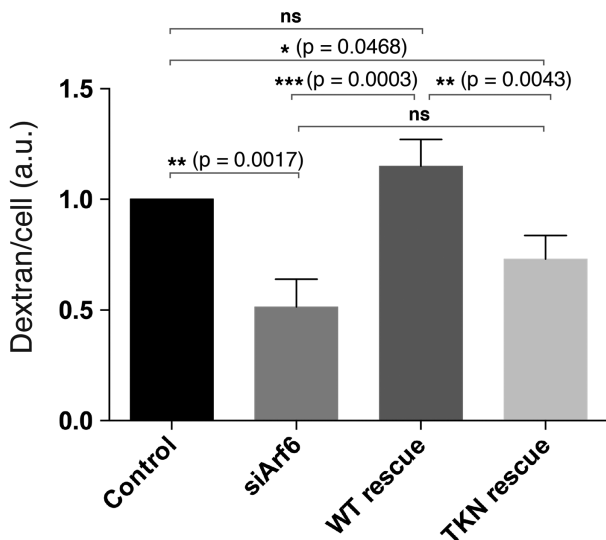
FIGURE 6: Expression of Arf6, but not the JIP-binding defective mutant of Arf6, rescues macropinocytosis in Arf6-depleted cells. HT1080 cells were seeded to six-well plates and either left untreated (control) or depleted for Arf6 with siRNA for 48 h. Subsequently, control cells were transfected with GFP vector and Arf6-depleted cells were either untransfected or transfected with siRNA-resistant forms of Arf6-GFP or Arf6TKN-GFP for 16–24 h. All sets of cells were then incubated with dextran-647 for 20 min, and dextran uptake was measured by flow cytometry. Bar graphs show the geometric mean dextran fluorescence of GFP-positive cells, reported as a fraction of control, from three separate experiments (GFP-positive cells were gated from a total of 100,000 cells per experiment). An ordinary one-way ANOVA was used to do a multiple comparison test between all groups, and a multiplicitiy adjusted *p* value is reported for each comparison. Error bars represent ± SD.

FIGURE 7: Model depicting macropinosome formation and transport. Sequential events in the macropinosome lifecycle are represented from PM ruffling, macropinosome formation, movement through the lamella, and into the cell interior (top to bottom of figure). Myosin IIA is present at the ruffling cell edge and myosin IIB is on the actin arc at the base of the lamella. Newly formed macropinosomes are coated in F-actin and myosin IIA and are often seen to compress as they move through the myosin IIB-associated actin arc prior to actin uncoating and release into the cell interior. Microtubules extend outward into the lamella (dashed lines), providing a tract for the incoming macropinosome through the lamellar actin mesh. Active Arf6 is present at the PM and recruits JIP3/4 to the forming macropinosome to engage a dynein motor for completion of macropinocytosis and transport into the cell interior. Two types of CIE cargo are illustrated (MHCI/CD59 and CD98/CD147).

It is well established that the actin cytoskeleton is important for the shaping of the membrane ruffles that fuse to form the macropinosome (Swanson, 2008; Bohdanowicz and Grinstein, 2013). At the same time, the dense actin filament network in the lamella could pose a barrier for macropinosome movement into the cell interior. The lamella is an actin- and myosin-rich region with myosin contractility facilitating actin retrograde flow and the formation of the actin arc (Burnette *et al.*, 2011), a barrier through which the macropinosome must pass. We observed distinct localization of endogenous myosin IIA to the PM edge and to macropinosomes, whereas myosin IIB was mostly present at the actin arc, defining the base of the lamella. This distribution fits well with previous reports (Maupin *et al.*, 1994; Kolega, 1998) and with the differing duty ratios of these nonmuscle myosin II isoforms (O'Connell *et al.*, 2007). Others have reported roles for myosin IIA in protrusions (Rai *et al.*, 2017), regulation of actin retrograde flow (Cai *et al.*, 2006), and circular ruffle formation that leads to macropinocytosis (Casalou *et al.*, 2014). Myosin IIB, alternatively, has been reported to generate tension at the base

of the lamella to act as a brake on retrograde flow (Brown and Bridgman, 2003; O'Connell *et al.*, 2007) and control protrusion stability (Lo *et al.*, 2004). Importantly, however, broad inhibition of myosin IIs with blebbistatin significantly inhibited macropinocytosis. In HT1080 cells, the interplay of these myosins may establish opposing

fluorescence from 240 individual cells per condition in a single matched experiment, error bars show the standard error of the mean. Experiments were repeated three times with similar phenotypes. An ordinary one-way ANOVA was used to compare groups to the NT control. *****p* value < 0.0001. (D) The extent of siRNA knockdown of JIP3, JIP4, JIP3 and JIP4, and Arf6 was assessed by Western blot of JIP4 and Arf6. (E) HT1080 cells depleted by siRNA of nontargeting control (Supplemental Movie 5), JIP3 (Supplemental Movie 6), or Arf6 (Supplemental Movie 7) were incubated with Alexa488–conjugated primary antibodies against CD147 for 1 h prior to live-cell imaging. Membrane ruffling and macropinocytosis were followed in live-cell imaging over the course of 20 min.
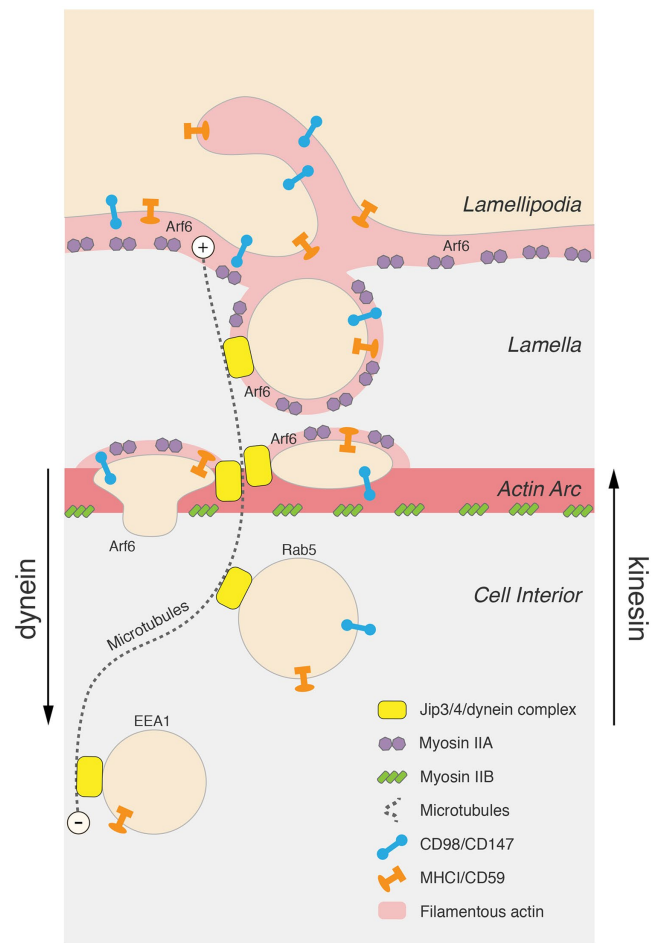
forces on a newly formed macropinosome to account for the dramatic deformation of the macropinosome as it moves through the actin-rich lamella. As the macropinosome squeezes through the actin arc, it loses both f-actin coating and myosin IIA. Exactly how this release occurs is not known but may involve changes in Arf6 GTP status and phosphoinositides on the macropinosome membrane.

Our data show that pioneering microtubules that extend out into the actin/myosin-enriched lamellae are required for the formation of the macropinosome. The dramatic loss of macropinosome formation on microtubule disruption (see Figure 3) raises the possibility that microtubules may deliver components to the cell surface needed for shaping cortical actin ruffles into macropinosomes. Such components could be delivered through endosomal recycling, a microtubule-dependent process (Delevoye et al., 2014). For example, a recent study reports that K-Ras–driven macropinocytosis in pancreatic cancer cells requires syndecan 1 recycling (Yao et al., 2019), a process shown to be dependent on Arf6 (Zimmermann et al., 2005). Consistent with our findings, phorbol ester- (Kruth et al., 2005) and M-CSF- (Racoosin and Swanson, 1989, 1992) stimulated macropinocytosis in macrophages were also inhibited by microtubule disruption.

Microtubules provide a track for the incoming macropinosome to travel on and move inward directed by dynein motor assembled onto the macropinosome by the JIP3/4 scaffold proteins. In addition to observing microtubules and endogenous dynein in the lamellae and in contact with nascent macropinosomes, inhibitors of dynein or depletion of JIP3, JIP4, or Arf6 inhibited macropinocytosis. The JIP proteins are scaffolds that bind to both kinesin and dynein (Fu and Holzbaur, 2014) and are thought to facilitate bidirection transport of endosomes. Arf6 binds to the leucine zipper II motif on both JIP3 and JIP4 (Isabet et al., 2009), and this interaction has been implicated in the regulation of fast endosomal recycling (Montagnac et al., 2011) and endosomal movement during mitosis (Montagnac et al., 2009). Although the exact effect that Arf6 binding to JIP3/4 has on kinesin versus dynein motor activity is not settled (Fu and Holzbaur, 2014), we observed Arf6 and JIP3/4 to be critical for macropinocytosis at a stage where dynein activity is also required. This would suggest that Arf6 is recruiting JIP3/4 to the macropinosome membrane to enable coupling to a dynein motor. Consistent with this, in cells depleted of Arf6, the cells continued ruffling and attempted, but could not complete, macropinocytosis (Figure 5E), a block similar to that observed in cells acutely treated dynein inhibitors, Ciliobrevin or dynarrestin (Figure 4, C and E).

Furthermore, we found that the Arf6 requirement for macropinocytosis required the interaction between Arf6 and JIP since an effector domain mutant of Arf6 (TKN) could not rescue macropinocytosis in Arf6-depleted cells, whereas wild-type Arf6 could. This suggests that the macropinocytosis requirement for Arf6 is for the recruitment and engagement of JIP and dynein and not for the stimulation of phosphatidylinositol 4-phosphate 5-kinase since the Arf6TKN mutant can still bind to, and presumably activate, the kinase (Suzuki et al., 2010). Nevertheless, there is a clear requirement for phosphoinositides, in particular the activity of PI-3 kinase for completion of micropinocytosis, as shown by Araki et al. (1996). Furthermore, the inhibition of PI-3 kinase did not affect membrane ruffling but blocked closure (Araki et al., 1996), a block similar to what we observed with inhibition of dynein or depletion of Arf6 or JIP3/4.

The role of JIP3/4 in forming and bringing the macropinosome into the cell interior using a dynein motor brings to mind the role described for JIP3, also known as Sunday Driver in Drosophila. JIP3 is involved in axonal clearance of large vesicles back to the cell body (Cavalli et al., 2005) and macropinosomes are essentially large

vesicles. Intriguingly, the addition of nocodazole to HeLa cells does not stop endocytosis, but halts endosomes in the cell periphery and blocks sorting of CIE cargo and maturation of CIE-derived endosomes (Maldonado-Baez et al., 2013). A unique role of microtubules and dynein, therefore, in endosome sealing and formation appears to be involved specifically in macropinocytosis. One interpretation of this observation is that the machinery for sorting is established during the initial formation of the macropinosome. Thus, the requirement for microtubules, dynein, and JIP3 in macropinosome formation ensures components for efficient recycling of the cargo from the macropinosome. As they pass through the actin arc barrier, macropinosomes lose their actin coat and begin the process of cargo sorting. The large size of the macropinosome will provide an excellent system to follow the process of cargo sorting during macropinosome maturation.

MATERIALS AND METHODS
Plasmids
GFP empty vector is from Invitrogen. Arf6 and Arf6T27N are in the pEGFP plasmid vector. The pmApple-N1-ITPKA (mApple-F-Tractin) was a gift from John Hammer (National Heart, Lung and Blood Institute [NHLBI]) and was described previously (Johnson and Schell, 2009; Beach et al., 2014). EMTB-3XGFP was a gift from William Bement (University of Wisconsin) (Addgene plasmid # 26741). GFP-Dynamin K44A was a gift from Mark McNiven (Mayo Clinic, Rochester, MN). GFP-N-Ras plasmid generation was previously described (Choy et al., 1999). RFP-farnesyl is the same as RFP-tH (Porat-Shliom et al., 2008).

Antibodies and fluorescent probes
Mouse monoclonal antibodies to MHCl (clone w6/32; immunoglobulin G [IgG]2a), CD98 (clone MEM-108; IgG1), and CD147 (clone HIM6; IgG1) were purchased from BioLegend (San Diego, CA) and used for immunofluorescence and antibody internalization assays at a 1:100 dilution (except anti-CD98, which was used at a 1:300 dilution). Rabbit anti-human nonmuscle myosin IIA antibodies (M8064) and rabbit anti-actin antibodies (clone A 2066) were purchased from Sigma and used for immunofluorescence at a 1:4000 dilution and Western blotting at a 1:5000 dilution, respectively. Mouse monoclonal antibodies to cytoplasmic dynein 1 intermediate chain 1 were purchased from EMD Millipore (Bethesda, MD) (MAB1618; IgG2b) and used for immunofluorescence at a 1:300 dilution (Rojas et al., 2008), and for immunofluorescence at a 1:500 dilution. Rabbit antibodies to Jip4 were purchased from Cell Signaling (D72F4) and used for Western blot at a 1:1000 dilution. Rabbit polyclonal antibodies to Arf6 (Song et al., 1998) were diluted 1:1000 for Western blots.

All secondary antibodies (Alexa Fluor 488–conjugated goat anti-mouse, Alexa Fluor 594–conjugated goat anti-mouse and goat anti-rabbit, Alexa Fluor 633–conjugated goat anti-rabbit, and Alexa Fluor 568–conjugated goat anti-rabbit) were used at a dilution of 1:750 (Invitrogen). Transferrin conjugated to Alexa Fluor 488 or 633 was purchased from Invitrogen and used at a 1:1000 dilution in internalization assays.

Zenon Alexa Fluor 488 Mouse IgG1 and Zenon Alexa Fluor 594 Mouse IgG1 labeling kits, purchased from ThermoFisher Scientific, were used where indicated to fluorescently label primary antibodies to CIE cargo for live-cell imaging, according to manufacturer's instructions. Rhodamine Phalloidin (Molecular Probes/Invitrogen) and Alexa Fluor 647 Phalloidin (Cell Signaling Technologies) were added to secondary antibody solutions at 1:200 and 1:20 final dilutions, respectively.

Other reagents

Nocodazole, Ciliobrevin D, jasplakinolide, cytochalasin D, and blebbistatin were purchased from Sigma-Aldrich. Dynarrestin was purchased from Probechem. Stock solutions for each of these chemicals were prepared in DMSO. For drug treatments reported here, DMSO vehicle controls were matched volumetrically to each drug, or to the drug having the lowest final dilution in media if a variety of treatments were compared in a single experiment. Saponin was purchased from Sigma-Aldrich. Poly-L-lysine solution (0.1% wt/vol) was purchased from Sigma-Aldrich.

Cell culture

HT1080 cells, obtained from the American Type Culture Collection, were maintained in EMEM supplemented with 10% fetal bovine serum (FBS), 100 U/ml penicillin, and 100 µg/ml streptomycin at 37°C with 5% CO_2. Cells were checked for mycoplasma every 6 mo. HeLa cells were maintained in DMEM supplemented with 10% FBS, 100 U/ml penicillin, and 100 µg/ml streptomycin at 37°C with 5% CO_2.

Electroporations, transfections, and siRNA treatment

HT1080 cells were transfected using Amaxa Nucleofector Kit T (Lonza). For each transfection, 1×10^6 cells were pelleted and resuspended in 100 µl room temperature Nucleofector Solution T. Two micrograms of total plasmid DNA was added, and cells were electroporated using Amaxa Program L-005 for high efficiency. Cells were transferred to either collagen-treated coverglass or untreated coverglass and incubated for 4–6 h before electroporation media were removed and cells were overlaid with fresh culture media. Cells plated onto collagen-treated coverglass were further processed 16–24 h after electroporation, while cells plated to untreated coverglass were further processed 72 h after electroporation. HeLa cells were plated the day before and then transfected the following day with Lipofectamine 2000, according to the manufacturer's instructions.

For siRNA transfections, four to five collagen-coated, circular 12-mm coverglasses (1.5 mm thickness) were added to a single well of a six-well plate and overlaid with a 1.5 ml solution containing 1×10^5 cells, 63 pmol siRNA, and 1.25 µl Lipofectamine RNAiMAX reagent (Invitrogen). Four to six hours later, media containing siRNA and Lipofectamine reagent were removed and fresh media overlaid on cells. Cells were incubated another 72 h before further processing. For Jip3, Jip4, and Arf6 depletions, we used ON-TARGETplus SMARTpool siRNA mixtures targeted against human gene sequences from Dharmacon. siRNA (63 pmol) was used for procedures with these SMARTpools. For Vps35 knockdown, we used 63 pmol of a single Qiagen siRNA oligo (Hs_VPS35_7) targeting the 5'-CAGAATTGCCCTTAAGACTTT-3' sequence (Varandas et al., 2016). For control siRNA, a nontargeting (NT) siRNA SMARTpool mixture from Dharmacon was used.

Dextran internalization measured by fluorescence imaging or flow cytometry

For fixed-cell dextran uptake assays, anionic, fixable AlexaFluor 594–conjugated 10 kDa dextran (Molecular Probes; D22913) was diluted to 333 µg/ml in culture media, or media/drug mixtures as indicated, and 100 µl of this solution was overlaid on a single 12-mm coverglass containing adherent cells and incubated for 20 min at 37°C. Cells were washed twice, quickly, in phosphate-buffered saline (PBS), pH 7.4, and then fixed for 10 min at RT in PBS plus 2% formaldehyde. Anionic, fixable AlexaFluor 488–conjugated 10 kDa dextran (Molecular Probes; D22910) was diluted as described above in serum-free culture media for the experiment comparing fluid

uptake in cells treated with Ciliobrevin or its concentration-matched DMSO vehicle, as Ciliobrevin D is inactivated by serum and also exhibits detectable autofluorescence in the red channel. After fixation, dextran-labeled cells were blocked with PBS supplemented with 10% FBS (PBS/FBS) for an hour, mounted to coverglass, and imaged within 12 h. Dextran appeared well immobilized against the macropinosome limiting membrane after fixation, but less so within the lumen of large macropinosomes particularly starting after 24 h postfixation. Dextran uptake images were acquired on Zeiss LSM880 using a 40× objective, with the pinhole open to its maximum setting, to capture all fluorescence within cells. Multiple 4×4 tile scans were acquired with 10% overlap. Images were stitched in Zeiss Zen software and then analyzed in Metamorph software (Molecular Devices). Individual cells were outlined in Metamorph and total fluorescent signal (in arbitrary fluorescence units) from single cells was collected. These values were transferred to Prism software for statistical analysis.

For live-cell dextran uptake assays, ~150,000 HT1080 untransfected or electroporated (where indicated) cells were seeded to each well of collagen-coated, six-well tissue culture plates (in siRNA experiments, cells were mock-treated or siRNA-treated for 48 h before trypsinizing, performing cell counts, and replating as above into collagen-coated plates). Two wells of cells were plated for each condition to be assayed. Twenty-four hours later, anionic, fixable AlexaFluor 647–conjugated 10 kDa dextran (Molecular Probes; D22914) was diluted to 40 µg/ml in culture media, or media/drug mixtures as indicated, and 0.5 ml of this solution was overlaid to each well of the six-well plate containing adherent cells and incubated for 20 min at 37°C. Dextran solution was promptly removed, and cells were washed once, quickly, in PBS, pH 7.4, before harvesting by trypsinization. Trypsin was inactivated with normal media and cells from replicate wells were combined and pelleted by centrifugation, ~1000 × g for 5 min. Media were removed and cell pellets were resuspended in 0.5 ml of ice-cold PBS, pH 7.4, and stored on ice. Cells were filtered using Cell-Strainer-capped 5-ml round-bottom tubes (Corning; 352235). A minimum of 100,000 cells per sample were analyzed using an LSRFortessa cell analyzer (BD Biosciences), gating for GFP-positive cells where indicated to compare transfected-cell populations. Data were analyzed using FlowJo software. Fluid internalization into cells was deduced by geometric mean intensity of Alexa Fluor 647.

Antibody and transferrin internalization

For antibody internalization techniques, cells were seeded to collagen-coated 12-mm circular 1.5-thickness coverglass, treated as described in the figure legends, and incubated with media containing antibodies to PM proteins at 37°C for various times to allow internalization. For chase experiments, after internalization cells were transferred to either fresh media or fresh media containing 25 mM NH_4Cl for times specified in figure legends. Where indicated for live-cell imaging, primary antibodies were directly conjugated to fluorophores using Zenon Antibody Labeling Kits (Molecular Probes), according to the manufacturer's instructions, prior to internalization into cells. Where indicated, cells were subjected to a 10–15-s wash in 0.5% acetic acid and 0.5 M NaCl (pH 3.0) to remove surface-bound antibody, then fixed in 2% formaldehyde in PBS for 10 min. Fixed cells were then rinsed in PBS followed by 1-h incubation in PBS supplemented with 10% FBS (PBS/FBS). Remaining antibodies exposed to the cell surface were blocked, where indicated, by incubation of unlabeled goat anti-mouse IgG antibodies (1:20 dilution; Jackson ImmunoResearch Laboratories) in PBS/FBS for 2 h at room temperature. Subsequent immunofluorescence used

standard protocols including 0.2% saponin for permeabilization. Coverslips were finally mounted on glass slides using Fluromount-G as mounting media (SouthernBiotech) and sealed with nail polish. For transferrin uptake, cells were washed in fresh culture media without serum for 30 min and then overlaid with serum-free media containing Alex Fluor 488 or 633–labeled transferrin for the indicated times and processed as above for immunofluorescence evaluation.

Immunofluorescence and imaging

Images were acquired using a Zeiss 780 laser scanning confocal microscope (63×, 1.4 NA PlanApo objective), a Zeiss 880 laser scanning confocal microscope (63×, 1.4NA PlanApo objective), or a GE DeltaVision OMX Microscope (60×, 1.42 NA objective). Raw SIM images were reconstructed using Softworx (Applied Precision), with a 3D SIM Weiner constant of 0.003 used for every frame of processing. After acquisition, images were handled using ImageJ and Adobe Photoshop. Statistical analyses were performed using Graphpad Prism (Graphpad Software). All scale bars in figures represent 5 μm, unless otherwise indicated.

Nikon Elements Software (NIS) was used to track macropinosome movement in Figure 1, defining macropinosome region perimeters with the fluorescent cargo (CD147) signal. Centroid positions of macropinosomes were calculated by NIS and velocity measurements interpolated by the software from centroid displacement between frames.

For live-cell imaging, HeLa or HT1080 cells were plated in Lab-Tek 1.5-thickness coverglass chambers, either untreated (HeLa cells) or treated with 5 μg/cm^2 collagen (HT1080 cells). Cells were imaged on a 37°C heated stage in normal growth media containing 25 mM HEPES, or in normal growth media with 5% CO_2 maintained by a CO_2 chamber.

REFERENCES

Amyere M, Payrastre B, Krause U, Van Der Smissen P, Veithen A, Courtoy PJ (2000). Constitutive macropinocytosis in oncogene-transformed fibroblasts depends on sequential permanent activation of phosphoinositide 3-kinase and phospholipase C. Mol Biol Cell 11, 3453–3467.

Araki N, Hatae T, Furukawa A, Swanson JA (2003). Phosphoinositide-3-kinase-independent contractile activities associated with Fcgamma-receptor-mediated phagocytosis and macropinocytosis in macrophages. J Cell Sci 116, 247–257.

Araki N, Johnson MT, Swanson JA (1996). A role for phosphoinositide 3-kinase in the completion of macropinocytosis and phagocytosis by macrophages. J Cell Biol 135, 1249–1260.

Bar-Sagi D, Feramisco JR (1986). Induction of membrane ruffling and fluid-phase pinocytosis in quiescent fibroblasts by ras proteins. Science 233, 1061–1068.

Beach JR, Shao L, Remmert K, Li D, Betzig E, Hammer JA 3rd (2014). Nonmuscle myosin II isoforms coassemble in living cells. Curr Biol 24, 1160–1166.

Bohdanowicz M, Grinstein S (2013). Role of phospholipids in endocytosis, phagocytosis, and macropinocytosis. Physiol Rev 93, 69–106.

Brown ME, Bridgman PC (2003). Retrograde flow rate is increased in growth cones from myosin IIB knockout mice. J Cell Sci 116, 1087–1094.

Buckley CM, King JS (2017). Drinking problems: mechanisms of macropinosome formation and maturation. FEBS J 284, 3778–3790.

Burnette DT, Manley S, Sengupta P, Sougrat R, Davidson MW, Kachar B, Lippincott-Schwartz J (2011). A role for actin arcs in the leading-edge advance of migrating cells. Nat Cell Biol 13, 371–381.

Cai Y, Biais N, Giannone G, Tanase M, Jiang G, Hofman JM, Wiggins CH, Silberzan P, Buguin A, Ladoux B, Sheetz MP (2006). Nonmuscle myosin IIA-dependent force inhibits cell spreading and drives F-actin flow. Biophys J 91, 3907–3920.

Casalou C, Seixas C, Portelinha A, Pintado P, Barros M, Ramalho JS, Lopes SS, Barral DC (2014). Arl13b and the non-muscle myosin heavy chain IIA are required for circular dorsal ruffle formation and cell migration. J Cell Sci 127, 2709–2722.

Cavalli V, Kujala P, Klumperman J, Goldstein LS (2005). Sunday Driver links axonal transport to damage signaling. J Cell Biol 168, 775–787.

Chaineau M, Ioannou MS, McPherson PS (2013). Rab35: GEFs, GAPs and effectors. Traffic 14, 1109–1117.

Chesneau L, Dambournet D, Machicoane M, Kouranti I, Fukuda M, Goud B, Echard A (2012). An ARF6/Rab35 GTPase cascade for endocytic recycling and successful cytokinesis. Curr Biol 22, 147–153.

Choy E, Chiu VK, Silletti J, Feoktistov M, Morimoto T, Michaelson D, Ivanov IE, Philips MR (1999). Endomembrane trafficking of ras: the CAAX motif targets proteins to the ER and Golgi. Cell 98, 69–80.

Commisso C, Davidson SM, Soydaner-Azeloglu RG, Parker SJ, Kamphorst JJ, Hackett S, Grabocka E, Nofal M, Drebin JA, Thompson CB, et al. (2013). Macropinocytosis of protein is an amino acid supply route in Ras-transformed cells. Nature 497, 633–637.

Delevoye C, Miserey-Lenkei S, Montagnac G, Gilles-Marsens F, Paul-Gilloteaux P, Giordano F, Waharte F, Marks MS, Goud B, Raposo G (2014). Recycling endosome tubule morphogenesis from sorting endosomes requires the kinesin motor KIF13A. Cell Rep 6, 445–454.

Donaldson JG, Porat-Shliom N, Cohen LA (2009). Clathrin-independent endocytosis: a unique platform for cell signaling and PM remodeling. Cell Signal 21, 1–6.

Dutta D, Donaldson JG (2015). Sorting of clathrin-independent cargo proteins depends on rab35 delivered by clathrin-mediated endocytosis. Traffic 16, 994–1009.

Eyster CA, Higginson JD, Huebner R, Porat-Shliom N, Weigert R, Wu WW, Shen RF, Donaldson JG (2009). Discovery of new cargo proteins that enter cells through clathrin-independent endocytosis. Traffic 10, 590–599.

Faire K, Waterman-Storer CM, Gruber D, Masson D, Salmon ED, Bulinski JC (1999). E-MAP-115 (ensconsin) associates dynamically with microtubules in vivo and is not a physiological modulator of microtubule dynamics. J Cell Sci 112(Pt 23), 4243–4255.

Frittoli E, Palamidessi A, Pizzigoni A, Lanzetti L, Garre M, Troglio F, Troilo A, Fukuda M, Di Fiore PP, Scita G, Confalonieri S (2008). The primate-specific protein tbc1d3 is required for optimal macropinocytosis in a novel arf6-dependent pathway. Mol Biol Cell 19, 1304–1316.

Fu MM, Holzbaur EL (2014). Integrated regulation of motor-driven organelle transport by scaffolding proteins. Trends Cell Biol 24, 564–574.

Ha KD, Bidlingmaier SM, Liu B (2016). Macropinocytosis exploitation by cancers and cancer therapeutics. Front Physiol 7, 381.

Hacker U, Albrecht R, Maniak M (1997). Fluid-phase uptake by macropinocytosis in dictyostelium. J Cell Sci 110(Pt 2), 105–112.

Hoing S, Yeh TY, Baumann M, Martinez NE, Habenberger P, Kremer L, Drexler HCA, Kuchler P, Reinhardt C, Choidas A, et al. (2018). Dynarrestin, a novel inhibitor of cytoplasmic dynein. Cell Chem Biol 25, 357–369 e356.

Isabet T, Montagnac G, Regazzoni K, Raynal B, El Khadali F, England P, Franco M, Chavrier P, Houdusse A, Menetrey J (2009). The structural basis of Arf effector specificity: the crystal structure of ARF6 in a complex with JIP4. EMBO J 28, 2835–2845.

Jiang J, Kolpak AL, Bao ZZ (2010). Myosin IIB isoform plays an essential role in the formation of two distinct types of macropinosomes. Cytoskeleton 67, 32–42.

Johnson HW, Schell MJ (2009). Neuronal IP3 3-kinase is an F-actin-bundling protein: role in dendritic targeting and regulation of spine morphology. Mol Biol Cell 20, 5166–5180.

Kerr MC, Teasdale RD (2009). Defining macropinocytosis. Traffic 10, 364–371.

Kolega J (1998). Cytoplasmic dynamics of myosin IIA and IIB: spatial "sorting" of isoforms in locomoting cells. J Cell Sci 111(Pt 15), 2085–2095.

Kovacs M, Toth J, Hetenyi C, Malnasi-Csizmadia A, Sellers JR (2004). Mechanism of blebbistatin inhibition of myosin II. J Biol Chem 279, 35557–35563.

Kruth HS, Jones NL, Huang W, Zhao B, Ishii I, Chang J, Combs CA, Malide D, Zhang WY (2005). Macropinocytosis is the endocytic pathway that

mediates macrophage foam cell formation with native low density lipo-protein. J Biol Chem 280, 2352–2360.

Lo CM, Buxton DB, Chua GC, Dembo M, Adelstein RS, Wang YL (2004). Nonmuscle myosin IIb is involved in the guidance of fibroblast migration. Mol Biol Cell 15, 982–989.

Maldonado-Baez L, Cole NB, Kramer H, Donaldson JG (2013). Microtubule-dependent endosomal sorting of clathrin-independent cargo by Hook1. J Cell Biol 201, 233–247.

Marchesin V, Castro-Castro A, Lodillinsky C, Castagnino A, Cyrta J, Bonsang-Kitzis H, Fuhrmann L, Irondelle M, Infante E, Montagnac G, et al. (2015). ARF6-JIP3/4 regulate endosomal tubules for MT1-MMP exocytosis in cancer invasion. J Cell Biol 211, 339–358.

Maupin P, Phillips CL, Adelstein RS, Pollard TD (1994). Differential localization of myosin-II isozymes in human cultured cells and blood cells. J Cell Sci 107(Pt 11), 3077–3090.

Montagnac G, de Forges H, Smythe E, Gueudry C, Romao M, Salamero J, Chavrier P (2011). Decoupling of activation and effector binding underlies arf6 priming of fast endocytic recycling. Curr Biol 21, 574–579.

Montagnac G, Sibarita JB, Loubery S, Daviet L, Romao M, Raposo G, Chavrier P (2009). ARF6 Interacts with JIP4 to control a motor switch mechanism regulating endosome traffic in cytokinesis. Curr Biol 19, 184–195.

O'Connell CB, Tyska MJ, Mooseker MS (2007). Myosin at work: motor adaptations for a variety of cellular functions. Biochim Biophys Acta 1773, 615–630.

Porat-Shliom N, Kloog Y, Donaldson JG (2008). A unique platform for H-Ras signaling involving clathrin-independent endocytosis. Mol Biol Cell 19, 765–775.

Racoosin EL, Swanson JA (1989). Macrophage colony-stimulating factor (rM-CSF) stimulates pinocytosis in bone marrow-derived macrophages. J Exp Med 170, 1635–1648.

Racoosin EL, Swanson JA (1992). M-CSF-induced macropinocytosis increases solute endocytosis but not receptor-mediated endocytosis in mouse macrophages. J Cell Sci 102(Pt 4), 867–880.

Rai V, Thomas DG, Beach JR, Egelhoff TT (2017). Myosin IIA Heavy chain phosphorylation mediates adhesion maturation and protrusion in three dimensions. J Biol Chem 292, 3099–3111.

Rojas R, van Vlijmen T, Mardones GA, Prabhu Y, Rojas AL, Mohammed S, Heck AJ, Raposo G, van der Sluijs P, Bonifacino JS (2008). Regulation of retromer recruitment to endosomes by sequential action of Rab5 and Rab7. J Cell Biol 183, 513–526.

Roossien DH, Lamoureux P, Miller KE (2014). Cytoplasmic dynein pushes the cytoskeletal meshwork forward during axonal elongation. J Cell Sci 127, 3593–3602.

Song J, Khachikian Z, Radhakrishna H, Donaldson JG (1998). Localization of endogenous ARF6 to sites of cortical actin rearrangement and involvement of ARF6 in cell spreading. J Cell Sci 111(Pt 15), 2257–2267.

Suzuki A, Arikawa C, Kuwahara Y, Itoh K, Watanabe M, Watanabe H, Suzuki T, Funakoshi Y, Hasegawa H, Kanaho Y (2010). The scaffold protein JIP3 functions as a downstream effector of the small GTPase ARF6 to regulate neurite morphogenesis of cortical neurons. FEBS Lett 584, 2801–2806.

Swanson JA (2008). Shaping cups into phagosomes and macropinosomes. Nat Rev Mol Cell Biol 9, 639–649.

Swift LM, Asfour H, Posnack NG, Arutunyan A, Kay MW, Sarvazyan N (2012). Properties of blebbistatin for cardiac optical mapping and other imaging applications. Pflugers Arch 464, 503–512.

van der Bliek AM, Redelmeier TE, Damke H, Tisdale EJ, Meyerowitz EM, Schmid SL (1993). Mutations in human dynamin block an intermediate stage in coated vesicle formation. J Cell Biol 122, 553–563.

Varandas KC, Irannejad R, von Zastrow M (2016). Retromer endosome exit domains serve multiple trafficking destinations and regulate local G protein activation by GPCRs. Curr Biol 26, 3129–3142.

Veithen A, Cupers P, Baudhuin P, Courtoy PJ (1996). v-Src induces constitutive macropinocytosis in rat fibroblasts. J Cell Sci 109(Pt 8), 2005–2012.

Waterman-Storer CM, Salmon ED (1997). Actomyosin-based retrograde flow of microtubules in the lamella of migrating epithelial cells influences microtubule dynamic instability and turnover and is associated with microtubule breakage and treadmilling. J Cell Biol 139, 417–434.

West MA, Bretscher MS, Watts C (1989). Distinct endocytotic pathways in epidermal growth factor-stimulated human carcinoma A431 cells. J Cell Biol 109, 2731–2739.

Yao W, Rose JL, Wang W, Seth S, Jiang H, Taguchi A, Liu J, Yan L, Kapoor A, Hou P, et al. (2019). Syndecan 1 is a critical mediator of macropinocytosis in pancreatic cancer. Nature 568, 410–414.

Zimmermann P, Zhang Z, Degeest G, Mortier E, Leenaerts I, Coomans C, Schulz J, N'Kuli F, Courtoy PJ, David G (2005). Syndecan recycling is controlled by syntenin-PIP2 interaction and Arf6. Dev Cell 9, 377–388.

Zoncu R, Perera RM, Balkin DM, Pirruccello M, Toomre D, De Camilli P (2009). A phosphoinositide switch controls the maturation and signaling properties of APPL endosomes. Cell 136, 1110–1121.